THE JOURNAL OF PHYSICAL CHEMISTRY C

Article

pubs.acs.org/JPCC

Mechanistic Evidence for Sequential Displacement–Reduction Routes in the Synthesis of Pd–Au Clusters with Uniform Size and Clean Surfaces

Sebastian Kunz and Enrique Iglesia*

Chemical Sciences Division, E.O. Lawrence Berkeley National Laboratory, Berkeley, California 94720, United States

Department of Chemical Engineering, University of California, Berkeley, California 94720, United States

Supporting Information

ABSTRACT: Bimetallic Pd–Au clusters with $(Pd/Au)_{at}$ compositions of 0.5, 1.0, and 2.0 narrowly distributed in size were prepared using colloidal methods with reagents containing only C, H, and O atoms, specifically polyvinyl alcohol (PVA) as protecting species and ethanol as the organic reductant. Synthesis protocols involved contacting a solution of Au precursors with nearly monodisperse Pd clusters. The formation of Pd–Au clusters was inferred from the monotonic growth of clusters with increasing Au content and confirmed by the in situ detection of Au plasmon bands in their UV–visible spectra during synthesis. Specifically, transmission electron microscopy (TEM) showed that growth rates were proportional to the surface area of the clusters, and rigorous deconvolution and background subtraction allowed for determination of the intensity and energy of Au-derived plasmon bands. This feature emerged during initial contact between Au precursors and Pd clusters apparently because Au^{3+} species deposit as Au^0 using Pd^0 as the reductant in a fast galvanic displacement process consistent with their respective redox potentials. The plasmon band ultimately disappeared as a result of the subsequent slower reduction of the displaced Pd^{2+} species by ethanol and of their deposition onto the bimetallic clusters. Such displacement–reduction pathways are consistent with the thermodynamic redox tendencies of Au, Pd, and ethanol and lead to the conclusion that such triads (two metals and an organic reductant) can be chosen from thermodynamic data and applied generally to the synthesis of bimetallic clusters with other compositions. These bimetallic clusters were dispersed on mesoporous γ-Al_2O_3 supports, and PVA was removed by treatment in ozone at near-ambient temperature without any detectable changes in cluster size. The absence of strongly bound heteroatoms, ubiquitous in many other colloidal synthesis protocols, led to Al_2O_3-dispersed clusters with chemisorption uptakes consistent with their TEM-derived cluster size, thus demonstrating that cluster surfaces are accessible and free of synthetic debris. The infrared spectra of chemisorbed CO indicated that both Pd and Au were present at such clean surfaces but that any core–shell intracluster structure conferred by synthesis was rapidly destroyed by adsorption of catalytically relevant species, even at ambient temperature; this merely reflects the thermodynamic tendency and kinetic ability of an element to segregate and to decrease surface energies when it binds an adsorbate more strongly than another element in bimetallic particles.

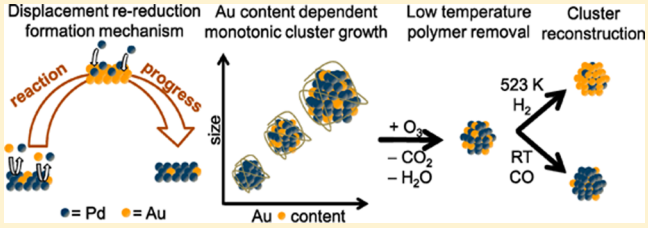

1. INTRODUCTION

Bimetallic nanoparticles have been ubiquitous in the industrial practice of heterogeneous catalysis since early studies of their unprecedented selectivity and stability in catalytic reforming processes that improve the octane of motor fuels through changes in their molecular composition instead of the use of toxic additives.[1] Bimetallic clusters are also the catalysts of choice in NO_x reduction and CO oxidation processes required for emissions control[2,3] and as electrodes in methanol and H_2 fuel cells.[4] The effects of alloying are typically discussed in terms of electronic (ligand) or geometric (ensemble) effects, albeit somewhat imprecisely.[5] Ligand effects capture the manner by which the local electronic properties of an atom sense the presence of vicinal atoms of another element. Ensemble effects result when a less active metal is assumed to dilute contiguous atoms of the more active element, thus decreasing the size of domains with homogeneous composition. Such catalytic consequences of alloying have also been described in terms of lattice mismatch and concomitant changes in the location and breadth of the d-bands in response to atomic displacements that perturb orbital overlap;[6] these latter proposals tend to erase the often arbitrary distinctions between geometry and electronics in bimetallic systems. Clearly, all these effects, irrespective of nomenclature or attribution, occur in concert; they are connected by the inseparable nature of atomic positions and electron configurations for any given element within a bimetallic cluster.

Received: January 16, 2014
Revised: March 8, 2014
Published: March 27, 2014

The interpretation of the catalytic consequences of atomic mixing requires bimetallic clusters of uniform size and chemical composition and exhibiting surfaces free of synthetic debris. Well-defined bimetallic structures can be prepared as extended surfaces of single crystals via vapor deposition,[7] but synthesis methods leading to well-defined catalytically relevant clusters have remained elusive. Impregnation and precipitation protocols can achieve bimetallic mixing only via subsequent thermal treatments, which often results in cluster growth through coalescence or Ostwald ripening that disrupts size and compositional uniformity.[8,9] Electroless deposition (ED) avoids such thermal treatments by depositing a second metal from an electroless bath onto the surface of pre-existing clusters,[10] but such methods are restricted to elements with precursor complexes stable against concurrent homogeneous nucleation of their monometallic clusters.[11]

Colloidal methods provide alternate routes to bimetallic clusters via either sequential or simultaneous reduction of mixed precursors in the presence of protecting surfactants, ligands, or polymers that inhibit coalescence[12−15] and can lead to bimetallic clusters with uniform composition.[16] These colloidal methods require protecting and reducing agents that tend to bind strongly to cluster surfaces (e.g., with S or B heteroatoms),[17,18] thus impairing the ultimate use of these materials as well-defined catalysts; such contaminated surfaces cannot be fully cleansed by subsequent treatments, which, even when effective, compromise the intended uniformity in size and composition.[19,20]

Here, we report protocols for the synthesis of bimetallic clusters using reagents containing only C, H, and O atoms with Pd−Au as a specific example of the general strategy proposed. Mechanistic inferences from in situ UV−visible spectra during synthesis and from transmission electron microscopy of the clusters formed confirmed that the formation of bimetallics involves displacement of the less noble element by the nobler one and the subsequent reduction of the displaced metals by the solvent. Such displacement−reduction sequences can occur in general for any pair of elements with different redox potentials.

These protocols are combined here with O_3 treatments after dispersing colloidal Pd and Pd−Au clusters on γ-Al_2O_3; such treatments remove protecting polymers at near-ambient temperatures without causing cluster coalescence or growth.[21,22] Even at ambient temperatures, the surface composition of Pd−Au clusters varied in response to the binding of adsorbates, a requirement for catalytic turnover. Segregation merely reflects the tendency of clusters to decrease their surface energy by placing the element that binds the adsorbates most strongly at their surfaces.[23,24] These findings confirm the ephemeral nature of core−shell structures and of any specific intracluster positional distribution of the two elements.[25] Spatial intracluster arrangements of the two elements are, in fact, determined by the contacting reactive media; any structures imposed by synthesis or thermal treatments are fully destroyed within a few catalytic turnovers, even at near-ambient temperatures.

2. EXPERIMENTAL METHODS

2.1. Preparation of Polyvinyl-alcohol (PVA)-Protected Pd, Au, and Bimetallic Pd−Au Clusters. *2.1.1. Preparation of Polyvinyl-alcohol (PVA)-Protected Pd Clusters.* Polyvinyl-alcohol (1.25 g PVA, Sigma Aldrich, 31 000−51 000 amu) was dissolved in a refluxing volumetric 1:1 ethanol (250 mL, EtOH, Sigma, >99.5%) and deionized water (resistivity ∼0.06 μS cm^{-1} in electrical conductivity) mixture at 373 K. The solution was cooled to ambient temperature, and 0.0333 g of $Pd(NO_3)_2 \cdot 2H_2O$ (Sigma Aldrich, ∼ 40% Pd) was added to obtain a Pd concentration of 5×10^{-4} mol L^{-1}. Cl-containing Pd precursors were avoided because they dissociate easily after dissolution in EtOH/H_2O mixtures in contrast to $Pd(NO_3)_2$. Such fast dissociation causes the immediate formation of solvated highly reducible Pd^{2+} species and the instantaneous formation of colloidal Pd clusters at ambient temperatures.[26] Monometallic Pd clusters cannot, as a result, be prepared in a controlled manner using Cl-containing Pd precursors in EtOH/H_2O media.

$Pd(NO_3)_2$ solutions (prepared as described above) changed from yellow to black when refluxed at 373 K (after ∼1.2 ks) in air, indicative of Pd cluster formation. Samples of 5 cm^3 were extracted every 1 h, cooled to ambient temperature, and examined by UV−visible spectroscopy, which detected no further changes in the spectra after 7 h, indicating that all reactions were complete.

2.1.2. Preparation of Polyvinyl-alcohol (PVA)-Protected Au Clusters. A solution of PVA was prepared by adding PVA (1.25 g) to a refluxing mixture of EtOH and deionized water (1:1 molar, 250 mL) and then cooled to ambient temperature. Chloroauric acid trihydrate ($HAuCl_4 \cdot 3H_2O$, Sigma Aldrich, 0.0491 g) was then added to give a metal concentration of 5×10^{-4} mol L^{-1}, and the mixture was stirred at ambient temperature for 12 h. Its color changed from yellow to clear during the first 6 h and thereafter to red, indicating the formation of colloidal Au particles.

2.1.3. Preparation of Polyvinyl-alcohol (PVA)-Protected Bimetallic Pd−Au Clusters. A $HAuCl_4 \cdot 3H_2O$ solution (0.0491 g, 5×10^{-4} mol Au L^{-1}) in a 1:1 mixture of EtOH/H_2O was added to a suspension of PVA-protected colloidal Pd (5×10^{-4} mol Pd L^{-1}, prepared as described in Section 2.1.1) at ambient temperature to give a final mixture with equimolar Pd and Au content ($(Pd/Au)_{at} = 1$). Different ratios of solutions and suspensions were used to obtain mixtures with 0.5 and 2 $(Pd/Au)_{at}$ ratios.

2.2. Elemental Composition of Bimetallic Clusters. Chemical compositions were measured by atomic absorption spectroscopy (AAS, Zeiss 5FL Flame). Clusters were precipitated by adding acetone (VWR, technical grade, 6 cm^3) to the suspension (4 mL). The solid residue was then isolated by centrifugation (Juergens Hettich EBA 3S, 100 s^{-1}, 0.6 ks), washed with acetone (VWR, technical grade, 10 mL) to remove any unreduced metal precursors ($Pd(NO_3)_2$ and $HAuCl_4 \cdot 3H_2O$ are both soluble in acetone), and kept in a vacuum desiccator for 1 h at <10 Pa (Vacuum Brand R5 rotary pump) to remove the solvent. The solids were dissolved in freshly prepared boiling aqua regia (2 mL), prepared from one aliquot HNO_3 (Sigma-Aldrich, ≥ 65%) and three aliquots HCl (VWR, 37%), for 600 s. Then aqua regia was added again and the solution boiled for a second time for 600 s. The clear solutions were cooled to ambient temperature, diluted with deionized water (to 25 mL volume), and analyzed by atomic absorption.

2.3. Ultraviolet−Visible Spectroscopy. UV−visible spectra of cluster suspensions were measured using quartz cuvettes and a two-beam spectrophotometer (Varian Cary 400 Bio). Spectra were collected with 5 nm s^{-1} scan rates in the 350−800 nm spectral range. Intensities below 350 nm were very high and frequently led to detector saturation. Time-dependent measure-

dx.doi.org/10.1021/jp500537v | J. Phys. Chem. C 2014, 118, 7468−7479

ments used Pd cluster suspensions (3 mL) (Section 2.1.1) within quartz cuvettes. Spectra were continuously acquired at 125 s intervals before and after adding freshly prepared solutions of Au precursors in 1:1 EtOH:H_2O mixtures (0.5 mL, 10^{-3} mol Au L^{-1}) to give a bulk $(Pd/Au)_{at}$ ratio of 1. After about 1.0 ks, no further spectral changes were detected, suggesting that the reaction was completed.

2.4. Cluster Deposition onto Porous Supports and Removal of Protecting Ligands. *2.4.1. Deposition of Clusters onto Porous Supports.* PVA-protected Pd and bimetallic ($(Pd/Au)_{at}$ = 0.5) clusters were adsorbed onto γ-Al_2O_3 (Sasol SBa-200, 150 m^2 g^{-1}) by adding 13.25 g (or 2.65 g) of γ-Al_2O_3 to 1:1 EtOH:H_2O suspensions of Pd clusters (250 mL) or Pd–Au clusters (150 mL, $(Pd/Au)_{at}$ = 0.5) to give metal contents of 0.1% wt (or 0.47% wt). These suspensions were stirred for 24 h at ambient temperature. Cluster deposition onto Al_2O_3 was evident from changes in color for the solids (white to brown) and the liquid (black to clear). Solids were recovered by filtration, washed twice with deionized water (5 mL g^{-1}), and treated in ambient air at 323 K for 12 h. UV–visible spectra of the filtrate and the supernatant solution before filtration were measured, confirming the absence of residual clusters in the suspension.

2.4.2. Removal of Protecting Polymer from Mono- and Bimetallic Clusters. The reaction of the protecting polymer with O_3 or O_2 was monitored by the rate of CO_2 evolution from clusters dispersed onto Al_2O_3 during temperature ramping (temperature-programmed reaction, TPR). Samples were pelleted, crushed, and sieved to retain aggregates 106–140 μm in diameter, which were then diluted with pure Al_2O_3 to prevent local temperature excursions during exothermic oxidation reactions. Samples were placed within a quartz tube equipped with a K-type thermocouple (Omega), and temperature was varied by resistive heating at a rate of 0.0833 K s^{-1} using a controlling device (Watlow Series 96 controller). These experiments used a mixture of pure O_2 (Praxair 99.999%, 30.9 cm^3 s^{-1} g^{-1}) in Ar (Praxair 99.999%, 1.2 cm^3 s^{-1} g^{-1}) with CO_2 (44 amu) and H_2O (18 amu) monitoring by mass spectrometry (Leybold Inficon Inc. Transpector Quadrupole). CO_2 and H_2O evolution profiles were identical for catalyst–support dilution ratios of 1:15 and 1:30 (catalyst:Al_2O_3 mass), consistent with the absence of any local temperature excursions. In some experiments, O_2/Ar mixtures were routed through a cold discharge O_3 generator (OzoneLab OL80) before contacting the samples to give an O_3 molar flow rate of 8.8×10^{-5} mol s^{-1} g^{-1} (as per manufacturer calibration).

2.5. Transmission Electron Microscopy. Transmission electron micrographs were obtained on samples placed on holey carbon Cu grids (Ted Pella Inc.) from suspensions of clusters in their synthesis medium or from acetone suspensions of such clusters on porous supports. A minimum of 500 clusters were measured for all samples using a JEOL 1200 EX microscope at an acceleration voltage of 80 kV.

2.6. Infrared Spectra of CO Chemisorbed on Al_2O_3-Supported Clusters. Infrared spectra were measured using a Thermo Nicolet 8700 spectrometer, an in situ flow cell,[27] and wafers (30 mg cm^{-2}) of Al_2O_3-supported samples. Wafers were treated with a flowing mixture of H_2 (11.1 H_2 cm^3 s^{-1} g^{-1}, Praxair 99.999%) and He (66.6 cm^3 s^{-1} g^{-1} He, Praxair 99.999%) by heating to 523 at 0.083 K s^{-1}, holding for 1 h, and cooling to 273 K using cold N_2. Samples were then exposed to a CO/He mixture (Praxair certified mixture; 7500 ppm CO, 5.55 cm^3 s^{-1} g^{-1}, 58 Pa CO; He, Praxair 99.999%, 66.6 cm^3 s^{-1} g^{-1}) at 273 K, heated to 323 at 0.033 K s^{-1}, and subsequently cooled again to 273 K. Infrared spectra were acquired at 273 K before and after intervening heating to 323 K.

2.7. Chemisorptive Titrations of Metal Atoms at Cluster Surfaces. *2.7.1. Titration of Strongly Bound Hydrogen by O_2.* Chemisorption uptakes were measured using a volumetric adsorption apparatus equipped with a Baratron gauge (1.33 kPa MKS) and a turbomolecular pumping system (Pfeiffer Vacuum, < 1 Pa dynamic vacuum). Al_2O_3-supported clusters were treated by heating at 0.083 K s^{-1} to 523 K, holding for 1 h in H_2 flow (Praxair 99.999%, 0.25 cm^3 s^{-1} g^{-1}) and evacuation at 523 K for 300 s before being cooled to 373 K. H_2 (Praxair 99.999%) was dosed at 1.2 kPa and 373 K for 60 s at 373 K to form a chemisorbed hydrogen monolayer, and the contacting gas phase was removed by evacuation for 0.6 ks at 373 K. The chemisorbed hydrogen monolayer was titrated with O_2 (Praxair 99.999%) at ambient temperature by measuring five-point O_2 isotherms in a pressure range of 0.1 to 1.2 kPa. An equilibration time of 0.42 ks was chosen for the first point and 0.18 ks for the following four points to achieve constant pressure for every measured point. O_2 uptakes (resulting from reaction with chemisorbed hydrogen and chemisorption onto sites vacated by hydrogen removal and water desorption) were determined by extrapolation of the five-point isotherms to zero pressure.[28] The reaction–adsorption stoichiometry is given by

$$1.33 \cdot Pd_{surface}H + O_2 \rightarrow Pd_{surface}O + 0.66 \cdot (H_2O)_{Ads.\,on\,Al_2O_3} \quad (2.1)$$

with H_2O scavenged by Al_2O_3 support to give a stoichiometry of 1 O_2 molecule per 1.33 Pd surface atoms.[28]

2.7.2. CO Chemisorption. CO chemisorption uptakes were measured volumetrically on Al_2O_3-supported samples using the apparatus described above. Five-point isotherms were measured in a range between 0.1 to 1.2 kPa CO (Praxair 99.999%) at ambient temperatures, and CO uptakes were estimated by extrapolation to zero pressure. Samples were heated at 0.083 K s^{-1} to 523 K and held for 1 h in H_2 (Praxair 99.999%, 0.25 cm^3 s^{-1} g^{-1}), evacuated to <1 Pa for 300 s, and cooled to ambient temperature. An equilibration time of 0.9 ks was chosen for the first point and 0.18 ks for the following four points to achieve constant pressure for every measured point. The adsorption stoichiometry was determined from the relative number of CO molecules adsorbed in bridge and linear configurations by integration of the corresponding IR absorption bands. The absorption coefficient for bridged CO was taken to be twice that of linear CO[29], and the two species were assumed to occupy two and one surface Pd atoms, respectively.[30] Using these approximations, a stoichiometry coefficient of 0.6 CO/Pd was determined for the monometallic Pd sample.

3. RESULTS AND DISCUSSION

3.1. Characterization and Formation Mechanism of Pd–Au Clusters. PVA-protected monometallic Pd clusters were prepared as described in Section 2.1.1 and used as the starting suspension to prepare bimetallic clusters with nominal $(Pd/Au)_{at}$ ratios of 0.5, 1.0, and 2.0 (see Section 2.1.3). Pd/Au ratios determined by atomic absorption spectroscopy (AAS, Table 1) agree well with the nominal compositions in the reagent solutions used, confirming the complete incorporation of metal precursors into the recovered solids. Representative transmission electron micrographs for Pd and Pd/Au clusters

dx.doi.org/10.1021/jp500537v | J. Phys. Chem. C 2014, 118, 7468–7479

Table 1. Chemical Bulk Composition Determined by Atomic Absorption Spectroscopy (AAS)[a]

	composition			
	Pd	$(Pd/Au)_{at}$ = 2	$(Pd/Au)_{at}$ = 1	$(Pd/Au)_{at}$ = 0.5
experimental surface-averaged diameter $\langle d \rangle$ (nm)	2.6 ± 0.7	2.7 ± 0.7	3.1 ± 0.7	3.9 ± 0.8
surface-averaged dispersity D_A	1.5	1.4	1.2	1.2
AAS composition	–	1.9	0.9	0.5
Δd_i (nm)	–	0.4	0.8	1.2
theoretical surface-averaged diameter $\langle d_{theo} \rangle$ (nm)	–	3.0	3.2	3.7
σ (%)	–	22	6	17
surface-averaged diameter $\langle d_{O_3} \rangle$ after O_3 treatment (nm)	3.1 ± 0.8	–	–	4.1 ± 0.8

[a]Surface-averaged diameters $\langle d \rangle$ and dispersities D_A determined from the particle size distributions. Δd_i and $\langle d_{theo} \rangle$ are the diameter increases and the surface-averaged diameters determined by a surface-average-dependent growth model (eq 3.9) and the Pd cluster size distribution (Figure 1a). σ (eq 3.10) quantifies the deviation of experimental and simulated histograms of bimetallic clusters modeled from the size distribution of the monometallic Pd clusters. $\langle d_{O_3} \rangle$ are the surface-averaged diameters of O_3-treated, supported clusters (89.6 kPa O_2, 6.7 kPa O_3, 3.7 kPa Ar, ambient temperature, 1 h).

with 0.5, 1, and 2 $(Pd/Au)_{at}$ ratios are shown in Figure 1, together with their cluster size distributions that exhibit a single sharp maximum.

Surface-averaged cluster diameters $\langle d \rangle$ are given by the equation

$$\langle d \rangle = \sum n_i d_i^3 / \sum n_i d_i^2 \quad (3.1)$$

where n_i is the number of clusters with a diameter of d_i. The $\langle d \rangle$ values for these clusters are shown in Table 1; diameters are 2.6 nm for monometallic Pd clusters and 2.7, 3.1, and 3.9 nm for bimetallics with $(Pd/Au)_{at}$ ratios of 2, 1, and 0.5, respectively. The size uniformity of these clusters can be described by a dispersity parameter D_A:[31]

$$D_A = \sum n_i \sum (\pi d_i^2)^2 n_i / (\sum \pi d_i^2 n_i)^2 \quad (3.2)$$

The values of D_A are 1.2–1.5 for all Pd and Pd–Au samples (Table 1). These values are near unity, the value expected for clusters of unimodal size. D_A values have not been widely reported for colloidal nanoparticles, in spite of IUPAC recommendations;[32] therefore, we also report standard deviations for mean diameters in Table 1. These standard deviations (15–30%) are typical of clusters prepared by using $NaBH_4$ reductants[33,34] but which tend to retain B and Na heteroatoms at cluster surfaces.

Size histograms (insets in Figure 1a–d for monometallic Pd and bimetallic clusters with nominal $(Pd/Au)_{at}$ compositions of 2, 1, and 0.5, respectively) show that the mean cluster size increased monotonically with increasing amounts of Au precursor added from 2.7 nm for clusters with a nominal $(Pd/Au)_{at}$ ratio of 2 (Figure 1b) to 3.9 nm for $(Pd/Au)_{at}$ ratios of 0.5 (Figure 1d). The monometallic Au clusters that formed by ethanol reduction in the absence of Pd clusters (Section 2.1.2) were much larger (10–20 nm, Figure S1 of Supporting Information) than these bimetallic Pd–Au clusters (Figure 1b–d). The micrographs of bimetallic clusters do not show any evidence for large clusters, which would have been expected from the independent reduction and nucleation of Au species. We conclude that Au precursors preferentially reacted with preexisting Pd clusters instead of forming separate Au nuclei. Such preferential deposition is consistent with the monotonic cluster growth observed with increasing Au content and with the absence of large monometallic Au clusters.

The mixing of Au and Pd within clusters can be probed using the unique UV–visible spectral features of Au-based systems,[35] for which electronic transitions within the valence band allow collective oscillations giving rise to a (plasmon) resonance in the visible range.[36] Classical scattering theory predicts that this band would shift to lower wavelengths with decreasing Au cluster size,[37,38] but plasmon band shifts can also be caused by the binding of molecules and by changes in the dielectric constant of the surrounding media.[39]

Typical UV–visible spectra for pure Au clusters prepared using our synthesis protocols (Section 2.1.2) (10–20 nm; TEM image in Figure S1 of Supporting Information) are shown in Figure 2 (●●●). The maximum of the plasmon band appears at 545 nm, as expected for large (10–100 nm) Au clusters.[39,40] Clusters of d-metal, such as Pd (Figure 2, –●–), do not exhibit plasmon bands in the visible range because resonances are damped by electron relaxation and interband transitions.[36] Such metals show instead an exponential decrease in absorption intensity with increasing wavelength.[34] These spectral differences between Pd and Au allow the detection of Au deposition and of intermetallic mixing during the process of colloidal synthesis. Separate Au clusters formed in the presence of Pd clusters by homogeneous nucleation of the Au precursors would be detectable by spectra consisting of the superimposed spectra for separate monometallic Pd and Au clusters.[35] Au plasmon resonances were indeed evident in samples prepared by physically mixing equimolar amounts of Pd and Au as separate monometallic colloidal particles (Figure 2, ———, $(Pd/Au)_{at}$ =1); for such mixtures, Pd clusters merely shift the plasmon band to slightly lower wavelengths, a result of a visual artifact brought forth by the superimposed Pd background.

The addition of Au precursors to preexisting Pd clusters (Section 2.1.3) did not lead to the appearance of a plasmon band (Figure 2, solid line), indicating that monometallic Au clusters did not form even though atomic absorption spectroscopy (AAS) of the recovered solids showed that Au precursors formed solids at these conditions (Table 1). In contrast, Pd clusters after addition of Au precursors gave spectra (Figure 2, solid line) characteristic of monometallic Pd clusters (Figure 2, –●–), consistent with previous findings for colloidal bimetallic Pd–Au clusters protected by dendrimers or other polymers (e.g., PVP).[34,35] We conclude from these UV–visible spectra that Au precursors react with preexisting Pd clusters to form bimetallic clusters without concurrent formation of monometallic Au clusters.

The monotonic increase in cluster size with increasing Au content indicates that reduction of Au^{3+} by ethanol and heterogeneous nucleation of Au^0 onto Pd clusters causes the formation of bimetallic clusters in a process previously denoted as a sequential reduction mechanism.[13] Another plausible route is the galvanic displacement of Pd by Au cations, induced by their different standard electrochemical potentials ($Pd^{2+} + 2e^- \rightarrow Pd$, 0.951 V; $Au^{3+} + 3e^- \rightarrow Au$, 1.498 V), with subsequent rereduction of displaced Pd^{2+} cations by ethanol and deposition onto the Au–Pd clusters.

dx.doi.org/10.1021/jp500537v | J. Phys. Chem. C 2014, 118, 7468–7479

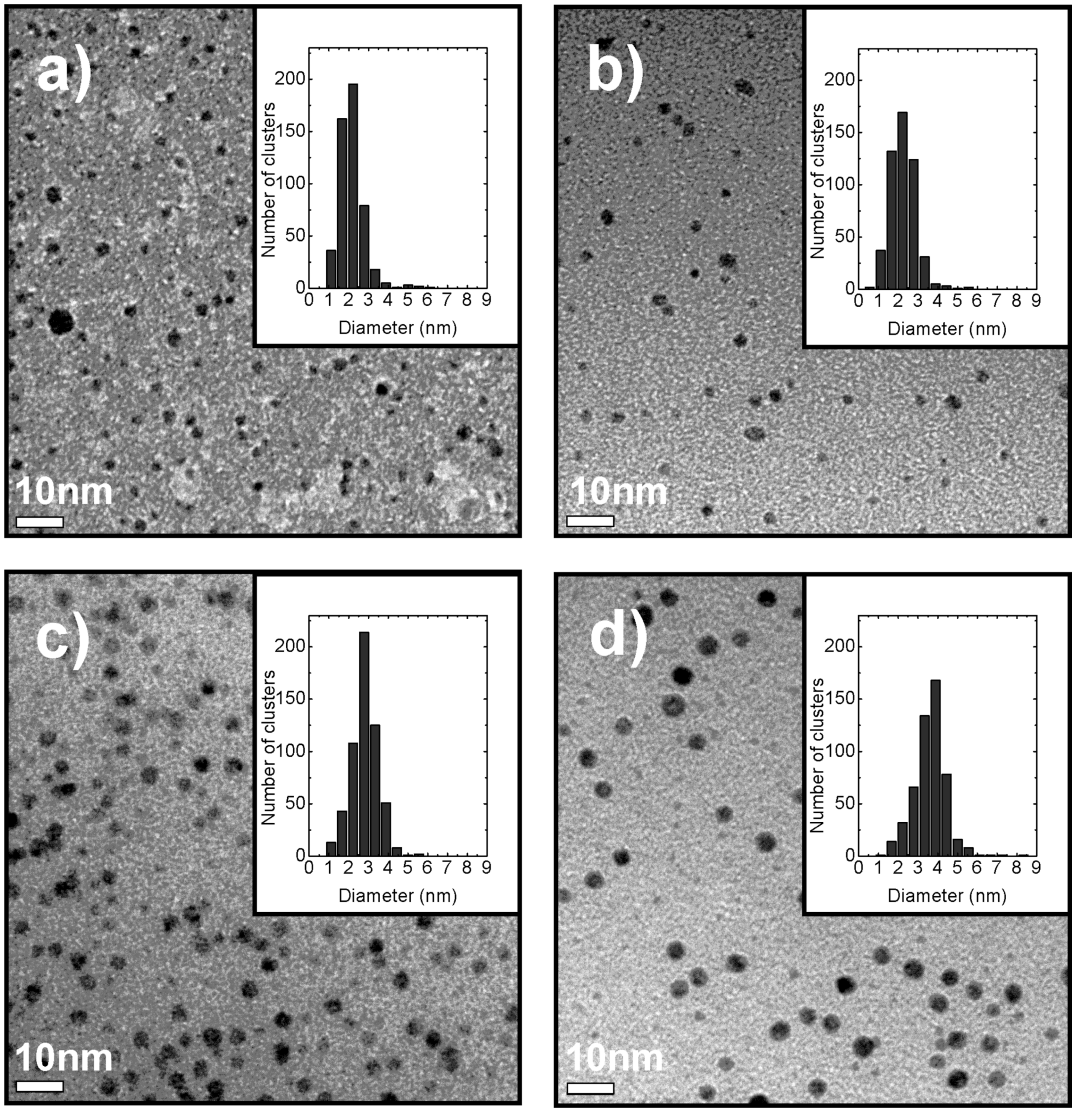

Figure 1. Transmission electron micrographs of monometallic Pd clusters (a) and three Pd–Au bimetallic compositions: $(Pd/Au)_{at}$ = 2 (b), $(Pd/Au)_{at}$ = 1 (c), and $(Pd/Au)_{at}$ = 0.5 (d).

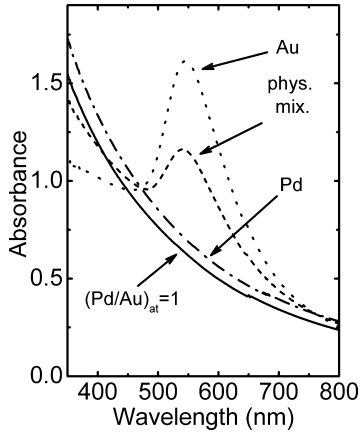

Figure 2. UV–visible absorption spectra of monometallic Pd clusters (–●–), monometallic Au (●●●), a physical mixture of monometallic Pd and monometallic Au clusters (– – –), and bimetallic $(Pd/Au)_{at}$ = 1 clusters (solid line).

The sequential reduction mechanism postulates the formation of an Au shell around a Pd core leading to a $Pd_{core}Au_{shell}$ structure with Au-like absorption properties that exhibits a pronounced plasmon resonance in the visible range.[41] This formation mechanism is inconsistent with our results because no plasmon band was found in the absorption spectra of our bimetallic clusters when the reaction was complete (Figure 2, –●–). Our synthesis protocols use excess ethanol as a reductant and polyvinyl-alcohol to prevent cluster coalescence; these alcohols, in contrast with strongly binding amines and thiols, do not induce fast reconstruction of core–shell bimetallic $Pd_{core}Au_{shell}$ clusters, a process that would disrupt any Au shells and eliminate plasmon bands.[41] The reduction of Au^{3+} precursors by ethanol at ambient temperatures, required for heterogeneous nucleation of Au^0 species, occurred much more slowly (>25 ks, Section 2.1.2) in the absence than in the presence of Pd clusters. In contrast, preexisting Pd clusters led to complete reduction of the Au precursors in ~1 ks (Section 2.3), suggesting that Pd clusters act as more effective reductants than ethanol for converting the Au precursor to Au^0, even when the latter is present in large excess within synthesis mixtures.

dx.doi.org/10.1021/jp500537v | J. Phys. Chem. C 2014, 118, 7468–7479

Thus, we conclude that Pd clusters are, in fact, the preferred reductant and that galvanic displacement of Pd^0 by Au^{3+} accounts for the bimetallic mixing achieved by these synthetic protocols. In this case, Pd metal atoms at the cluster surface are displaced by Au (Figure 3, step 1).[42] The concentration of H_2O is 10^4–10^5 times higher than that of the anions of the precursor salts (Cl^- and NO_3^-, both in the range of 10^{-3} to 10^{-4} M), making it likely that displaced atoms exist predominantly as solvated Pd^{2+} ions. The rate of reduction of solvated Pd^{2+} ions by ethanol at ambient temperature is about 100-fold higher than that of the Au precursor used ($HAuCl_4$), as reported by Yonezawa et al.[26] Thus, solvated Pd^{2+} ions are reduced rapidly by ethanol and are redeposited onto the Au shell of the bimetallic clusters (Figure 3, step 2), leading to the monotonic growth with increasing Au content and the absence of a plasmon resonance observed for these clusters.

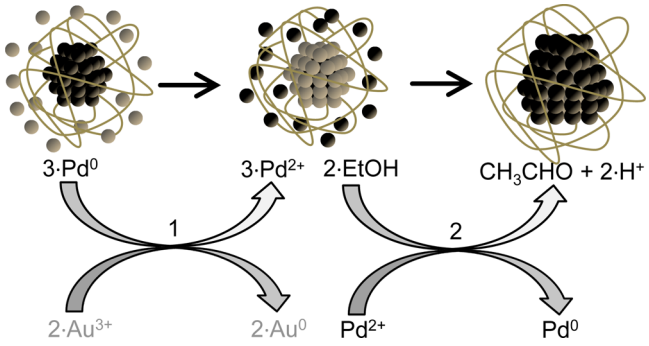

Figure 3. Sequential two-step reduction mechanism for bimetallic Pd–Au cluster formation from Pd clusters. In the first step, PVA-protected Pd clusters undergo galvanic displacement by Au^{3+} precursors, with concurrent reduction and deposition of Au and oxidation and dissolution of Pd^{2+}. In the second step, the Pd^{2+} formed is reduced by ethanol and deposits as Pd^0 onto the cluster.

In situ UV–visible spectra are shown in Figure 4 for (i) the initial colloidal suspension of Pd clusters (●●●), (ii) this sample 0.18 ks after adding the Au^{3+} precursor solution (– – –), and (iii) this sample after 1.02 ks (no changes were detected thereafter) (solid line). The initial colloidal suspension showed the exponential decay with increasing wavelength characteristic of Pd metal clusters (the gray line in Figure 4 is a regressed exponential fit for the Pd cluster spectrum).[36] A small shoulder at 450–600 nm appears after adding the Au precursors (Figure 4, – – – spectrum); this feature is absent in Pd and Au precursors and corresponds to a plasmon band that is characteristic of clusters exposing Au^0 surfaces. These data indicate that such surfaces incipiently form during the initial contact of Pd clusters with Au precursors. The spectrum can be fitted with an exponential function (Figure 4, solid gray line on – – – spectrum) for the range of wavelengths that excludes the plasmon resonance (450–600 nm); this background was then subtracted from the spectra of bimetallic clusters as a function of synthesis time to obtain the specific features associated with the Au species deposited (inset in Figure 4).

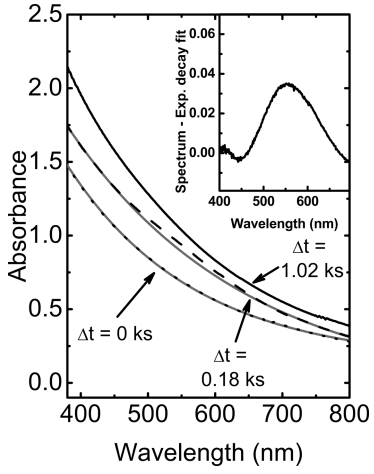

Figure 4. UV–visible absorption spectra for monometallic Pd clusters (●●●), monometallic Pd clusters 0.18 ks after adding Au precursors (– – –), and bimetallic $(Pd/Au)_{at}$ = 1 clusters (1.02 ks after injection of the precursor) after which no further changes were observed (solid line). The inset in the top right corner shows the plasmon resonance extracted for the spectrum recorded during the reaction (– – –).

This procedure enabled measurements of the intensity (Figure 5a) and wavelength of the plasmon bands (Figure 5b) as displacement and reduction occurred during synthesis. The plasmon band appeared immediately after introduction of the Au^{3+} solution; it became most intense after 0.48 ks (Figure 5a) and then weakened and reached a constant intensity after ~1.0 ks, indicating that the reaction was complete. The initial increase in the plasmon band intensity suggests that Pd cluster surfaces become covered, at least in part, by Au^0,[36] a process that we interpret as evidence of Au^0 deposition via galvanic displacement at Pd surfaces in the early stages of contact between Pd clusters and the Au^{3+} solution (Figure 3). These surfaces are subsequently enriched in Pd by the rereduction of the displaced Pd^{2+} cations by ethanol, which causes the observed decrease in the intensity of the plasmon resonance with time and results in an absorption spectrum that almost reflects the absorption properties of monometallic Pd clusters with only a small residual plasmon band remaining (Figure 4; solid, black line). The plasmon band maximum was initially at 560 nm but shifted to shorter wavelengths with reaction time during bimetallic cluster formation (Figure 5b) and then remained at 510 nm after 1.0 ks; no further changes were detected at longer times. For monometallic Au clusters, this shift would correspond to a decrease in cluster size from 10 to 100 nm,[40] but clusters in this size range were not detected in TEM images. The observed shift resembles that reported for bimetallic Pd–Au clusters prepared via reduction with polyols,

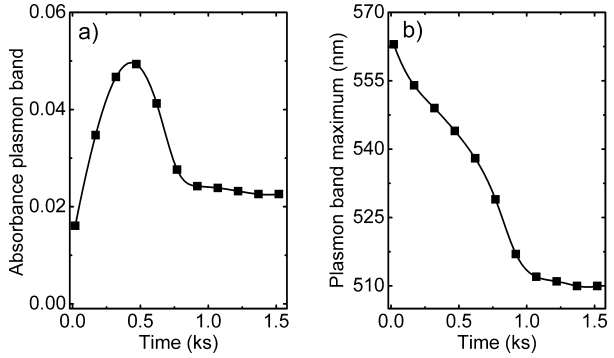

Figure 5. Evolution of the UV–visible spectra after introduction of Au^{3+} precursors into a suspension of monometallic Pd clusters at ambient temperature. (a) Plasmon resonance intensity ; (b) plasmon band absorption wavelength (curves represent trend lines).

dx.doi.org/10.1021/jp500537v | J. Phys. Chem. C 2014, 118, 7468–7479

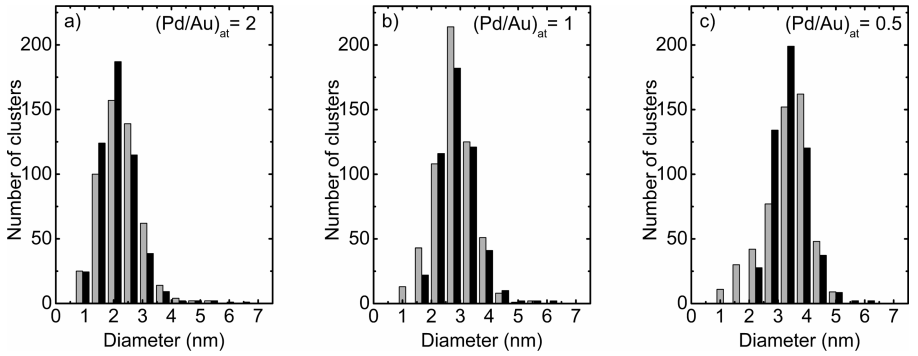

Figure 6. Particle size distributions of bimetallic Pd–Au clusters with $(Pd/Au)_{at}$ compositions of 2 (a),1 (b), and 0.5 (c) (gray, from TEM images; black, predicted from growth model and size distribution of initial Pd clusters; Section 3.1, eq 3.9).

which was attributed to Pd deposition onto Au surfaces through correlation with model calculations.[43] These in situ UV–visible spectra provide compelling evidence for the rapid (galvanic) displacement of surface Pd by Au, with subsequent rereduction of the displaced Pd^{2+} to Pd^0 and its deposition onto bimetallic Pd–Au clusters.

Next, we explore how this growth model leads to Pd–Au clusters of a given size after the deposition of a given amount of Au. The growth of a quasi-spherical particle i of a diameter d_i and containing n_i moles of atoms occurs at a rate proportional to its surface area A_i:

$$\frac{dn_i}{dt} = A_i k = \pi d_i^2 k \tag{3.3}$$

where k is the areal rate constant. The particle volume V_i is given by

$$V_i = n_i V_{i,M} = \frac{1}{6}\pi d_i^3 \tag{3.4}$$

where $V_{i,M}$ is the molar volume. Substituting for n_i in eq 3.3 gives

$$\frac{d(d_i)}{dt} = 2V_{i,M}k \tag{3.5}$$

For particles of an initial diameter $d_{i,0}$, the solution to eq 3.5 is

$$d_i(t) - d_{i,0} = \Delta d_i = 2V_{i,M}kt \tag{3.6}$$

indicating that all particles, irrespective of their initial size, increase in diameter (Δd_i) by the same amount in any given deposition time.[44,45] This treatment gives the expected size distribution of bimetallic clusters with a given Au content for any initial size distribution of preexisting Pd clusters.

The volume $V_{clusters}$ of $N_i(d_{i,0})$ clusters of a given size is determined by the summation of the product of the particle volumes ($v_{i,0}$) and the number of clusters $N_i(d_{i,0})$ with such a volume $v_{i,0}$:

$$V_{clusters}(N_i, d_{i,0}) = \sum_i N_i(d_{i,0})v_{i,0} = \sum_i N_i(d_{i,0})\frac{1}{6}\pi d_{i,0}^3 \tag{3.7}$$

Equation 3.7 was used to calculate the volume $V_{Pd\ clusters}(N_i,d_{i,0})$ of $N_i(d_{i,0})$ preexisting Pd clusters with the size distribution in Figure 1a. The volume $V_{Pd-Au\ clusters}$ (N_i, $d_{i,0}$ + Δd_i) of $N_i(d_{i,0} + \Delta d_i)$ bimetallic clusters formed by reaction of a given amount of Au precursors with $N_i(d_{i,0})$ preexisting Pd clusters is then given by

$$V_{Pd-Au\ clusters}(N_i, d_{i,0} + \Delta d_i) = V_{Pd\ clusters}(N_i, d_{i,0}) + V_{Pd\ clusters}(N_i, d_{i,0})\left(\frac{V_{M,Au}}{V_{M,Pd}}\right)\left(\frac{Au}{Pd}\right)_{at} \tag{3.8}$$

where $(V_{M,Pd}/V_{M,Au})$ is used to account for the different molar volumes of Pd and Au ($V_{M,Pd} = 8.54 \times 10^{-6}$ m^3 mol^{-1}, $V_{Au,M} = 10.21 \times 10^{-6}$ m^3 mol^{-1})[46] and $(Au/Pd)_{at}$ for the nominal metal ratio of the bimetallic clusters. The obtained $V_{Pd-Au\ clusters}$ (N_i, $d_{i,0}$ + Δd_i) values give the expected increase in diameter Δd_i, which is the same for all clusters irrespective of size (eq 3.6), via an iterative process

$$V_{Pd-Au\ clusters}(N_i, d_{i,0} + \Delta d_i) = \sum_i N_i(d_{i,0})\frac{1}{6}\pi(d_{i,0} + \Delta d_i)^3 \tag{3.9}$$

where N_i is the number of preexisting Pd clusters with initial diameter $d_{i,0}$ and Δd_i is the change in diameter for such clusters. The predicted size distribution for a given metal ratio $(Pd/Au)_{at}$ is then obtained by adding this change in diameter Δd_i to each $d_{i,0}$ in the initial Pd cluster size distribution, resulting in a Δd_i shift along the abscissa of the histogram.

The initial Pd cluster size distribution (Figure 1a) was used to determine the predicted Δd_i values for bimetallic clusters with $(Pd/Au)_{at}$ ratios of 0.5, 1, and 2, and the measured size distributions (Figure 1b–d) were normalized for comparison to the number of clusters of the initial Pd cluster ensemble. The predicted and measured distributions shown in Figure 6 agree well and accurately describe the observed shift to larger clusters with increasing Au content (bimetallic clusters with $(Pd/Au)_{at}$ ratios of 2, 1, and 0.5 are shown in Figure 6 a–c, respectively). Deviations between experiment and model, estimated using

$$\sigma = \frac{\sqrt{\sum_i (N_{i,theo}(d_i) - N_{i,exp}(d_i))^2}}{\sum_i N_{i,exp}(d_i)} \tag{3.10}$$

were between 6 and 22% (Table 1). The predicted surface-averaged diameters were 3.0, 3.3, and 3.7 nm for $(Pd/Au)_{at}$ ratios of 2, 1, and 0.5, respectively, in good agreement with measured values (2.7, 3.1, and 3.9 nm, respectively; Table 1). Thus, the assumption that galvanic deposition and rereduction rates proportional to cluster area seems consistent with the measured growth rates of bimetallic clusters formed by our synthesis protocol.

dx.doi.org/10.1021/jp500537v | J. Phys. Chem. C 2014, 118, 7468–7479

The chemical composition of a cluster grown at rates proportional to its surface area can be expressed using eq 3.4 to get eq 3.11

$$\frac{n_{Au}}{n_{Pd}} = \frac{\frac{1}{6}\pi({d_i}^3 - {d_{i,0}}^3)V_{M,Au}}{\frac{1}{6}\pi {d_{i,0}}^3 V_{M,Pd}} = \left(\frac{{d_i}^3}{{d_{i,0}}^3} - 1\right)\frac{V_{M,Au}}{V_{M,Pd}} \quad (3.11)$$

with $d_{i,0}$ the initial cluster diameter, d_i the diameter at a time t, and $V_{M,Pd}$ and $V_{M,Au}$ the molar volumes of Pd and Au, respectively. Substituting for d_i in eq 3.11 with eq 3.6 gives eq 3.12

$$\frac{n_{Au}}{n_{Pd}} = \left(\frac{(2ktV_{M,Au} + d_{i,0})^3}{{d_{i,0}}^3} - 1\right)\frac{V_{M,Au}}{V_{M,Pd}} \quad (3.12)$$

The initial diameter $d_{i,0}$ does not cancel out, showing that the chemical composition of a cluster at a time t depends on its initial diameter $d_{i,0}$. As a result, clusters of different size show different Au/Pd ratios and bimetallic clusters become compositionally uniform only when initial Pd clusters are uniform in size, a condition met, to a reasonable extent, by the Pd cluster suspensions in this study (Figure 1a).

The elementary steps involved in bimetallic cluster formation (Figure 3) are depicted in Scheme 1. The dissociation of the Au

Scheme 1. Elementary Steps of the Proposed Sequential Displacement–Reduction Mechanism for the Formation of Bimetallic Pd–Au Clusters

$$HAuCl_4 \xrightarrow{k_1} H^+ + AuCl_4^- \quad (1)$$

$$2AuCl_4^- + 3CH_3CH_2OH \xrightarrow{k_2} 2Au + 6H^+ + 8Cl^- + 3CH_3CHO \quad (2)$$

$$2AuCl_4^- + 3Pd_{Surface} \xrightarrow{k_3} 2Au_{Surface} + 8Cl^- + 3(Pd^{2+})_{solvated} \quad (3)$$

$$(Pd^{2+})_{solvated} + CH_3CH_2OH \xrightarrow{k_4} Pd^0_{solvated} + 2H^+ + CH_3CHO \quad (4)$$

$$Pd^0_{solvated} + Cluster \xrightarrow{k_5} Pd^0_{deposited\ on\ Cluster\ Surface} \quad (5)$$

precursors (step 1) is assumed to be fast and complete. Au^{3+} reduction to Au^0 by ethanol (step 2) was much slower when Pd^0 clusters were absent, indicating that the reduction of Au^{3+} by Pd^0 (step 3) is much faster than that by ethanol (step 2). The dependence of growth rates on cluster area suggests that step 3 or 5 limits rates of bimetallic cluster growth because they are the only steps that involve a cluster as a reactant. A kinetically relevant step 5 would lead to high Pd^0 concentrations, which would favor homogeneous nucleation and the formation of monometallic Pd clusters. In such instances, Pd–Au clusters would retain their plasmon band (instead of being covered by Pd).[41] In contrast, the spectra of the synthesis media after completing the reaction did not show a plasmon band (Figure 2), suggesting that step 3 is the sole kinetically relevant step. As a result, the dynamics and thermodynamics of cluster growth determine the viability and time scales of bimetallic formation. When Au clusters were used as preexisting clusters and the Pd precursor ($Pd(NO_3)$) was added, no reaction occurred at ambient temperature, as Au is more noble than Pd. Instead, the suspension had to be refluxed to achieve reduction of the Pd precursor via the solvent, which was accompanied by coalescence of the Au clusters to form a red solid precipitate that inhibited the formation of bimetallic Pd–Au clusters. Thermodynamics hence dictates that bimetallic particles will form only when clusters of the less noble metal are exposed to solvated precursors of the nobler metal, with deposition rates likely to be driven by their difference in electrochemical reduction potentials. Such conclusions provide general guidance for designing synthesis protocols for bimetallics other than the Pd–Au system chosen here as a specific example.

3.2. Removal of the Protective Polymer by Ozone Treatments. Monometallic and bimetallic clusters protected by polyvinyl-alcohol were adsorbed onto a mesoporous γ-Al_2O_3 support from colloidal suspensions by stirring for 24 h at ambient temperature. Adsorption was detected by changes in the colors of the solid support (white to brown) and the supernatant liquid (black to clear). The solids were recovered by filtration, and UV–visible spectra of the filtrate (Figure S3 of Supporting Information) did not detect the presence of any residual clusters that would lead to absorption spectra like the ones shown in Figure 2, only with lower absorbance.

The protecting polymers block access to metal surfaces and must be removed before catalytic use of these bimetallic clusters; the protocols required must not disrupt the size and compositional uniformity achieved during synthesis. Thermal treatments in H_2 or O_2 require high temperatures and cause cluster growth.[33] UV radiation leads to the formation of O_3 in oxygen atmospheres; O_3 then decomposes to form O radicals that can initiate the combustion of organic residues at near-ambient temperatures.[21,22] Here, we used a spark discharge O_3 generator to remove the protecting polymer at ambient temperature.

CO_2 formation rates are shown in Figure 7a for two supported monometallic PVA-protected Pd cluster samples

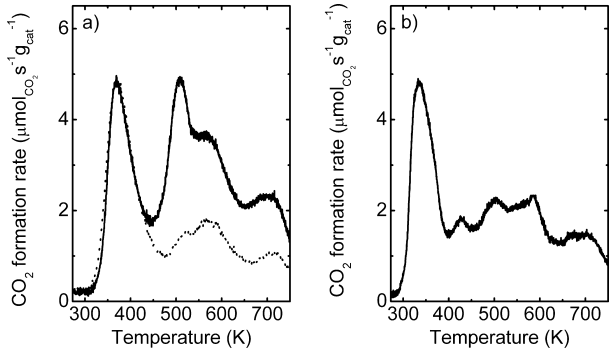

Figure 7. Temperature-dependent CO_2 evolution rates of untreated (solid line) and O_3-pretreated Pd (●●●) cluster samples (89.6 kPa O_2, 6.7 kPa O_3, 3.7 kPa Ar, ambient temperature, 1 h) in flowing O_2 (96.3 kPa O_2, 3.7 kPa Ar) (a). CO_2 evolution rates of a Pd cluster sample in a mixture of O_2/O_3/Ar (89.6 kPa O_2, 6.7 kPa O_3, 3.7 kPa Ar), which was previously treated in a flow of O_2 (96.3 kPa, 3.7 kPa Ar) at 400 K for 1 h to remove adsorbed CO_2 prior to the experiment (b). The CO_2 evolution below 400 K in (b) is hence related to PVA reacting with O_3. The integrated CO_2 evolution rates for (a) and (b) are shown in Figure S5 of Supporting Information.

(diluted to prevent local exotherms; 1:15 = catalyst:Al_2O_3) as a function of temperature in O_2 flow (96.3 kPa; Ar, 3.7 kPa as internal standard). One sample (solid curve) was not previously treated, while the other one (●●●) was treated at ambient temperature in an O_3-containing stream (96.3 kPa O_2; 2.0 kPa O_3 as per calibration) for 1 h. An experiment performed with pure Al_2O_3 in O_2 (96.3 kPa O_2, 3.7 kPa Ar) showed CO_2 evolution at 370 K (Figure S4a of Supporting Information) without additional features at higher temperatures. The same

dx.doi.org/10.1021/jp500537v | J. Phys. Chem. C 2014, 118, 7468–7479

experiment performed with PVA adsorbed on Al_2O_3 demonstrates that in the presence of PVA, CO_2 evolution occurs at temperatures above 450 K (Figure S4a of Supporting Information). Hence, we attribute the CO_2 peak at 370 K to desorption from Al_2O_3 and the features at higher temperatures to PVA decomposition. Three PVA decomposition features (510, 570, and 710 K) were found for the PVA-protected Pd clusters, irrespective of their pretreatment (Figure 7a), but the O_3-treated sample showed much smaller amounts of CO_2. Subtraction of the CO_2 desorption contribution of Al_2O_3 (solid line in Figure S4b of Supporting Information) from the integrated CO_2 evolution rates (Figure S5a of Supporting Information) shows that the CO_2 formed on O_3-treated samples was 0.42 of that from the untreated sample, consistent with significant removal of PVA by O_3 at ambient temperature and with the chemisorption data shown below.

The effect of O_3 treatment temperatures on PVA removal was probed by first treating supported Pd clusters in O_2 (96.3 kPa) and Ar (3.7 kPa) at 400 K until no CO_2 was detected in the effluent by mass spectrometry (~1 h). Then the sample was cooled to ambient temperature and the CO_2 evolution was measured by increasing the temperature while exposing this sample to flowing O_2 (89.6 kPa) and O_3 (6.7 kPa), with Ar as internal standard (3.7 kPa) (Figure 7b). CO_2 evolution first occurred at 335 K, which is lower than the temperature of its previous treatment in O_2 (400 K), indicating that this feature correspond to O_3 reaction with PVA (instead of CO_2 desorption from Al_2O_3 or O_2 reaction with PVA), thus confirming the reactivity of O_3 with the PVA polymer at near-ambient temperatures. PVA removal is not complete after O_3 treatment even though CO_2 removal rates decrease to undetectable levels above 400 K in the presence of O_3. Such incomplete removal may reflect (i) the removal of PVA vicinal to clusters, (ii) O_3 decomposition to O_2 as clusters become clean at higher temperatures, or (iii) concurrent pyrolysis reactions of PVA, which render these species less reactive in O_3-mediated reactions. Irrespective of the specific interpretation, matters of surface cleanliness remain the ultimate arbiter of treatment success in the use of these colloidal Pd and Pd–Au clusters as catalysts. Their catalytic properties in CO oxidation will be examined in a later study. Here, we examine next whether such treatments led to clean cluster surfaces or to cluster growth.

First, monometallic Pd and bimetallic clusters with a $(Pd/Au)_{at}$ ratio of 0.5 were adsorbed on Al_2O_3 and imaged by TEM. Surface-averaged diameters of 2.9 and 3.9 nm for adsorbed mono- and bimetallic clusters (Figure 8a,b), respectively, were essentially the same as the suspensions from which the particles were adsorbed onto Al_2O_3 (2.6 and 3.9 nm, respectively, Table 1), indicating that deposition did not cause detectable coalescence. Subsequent treatment of these supported clusters in O_3/O_2 mixtures at ambient temperatures led to very slight cluster growth (compare Figure 8a with Figure 8c and Figure 8b with Figure 8d; 2.9 to 3.1 nm for Pd; 3.9 to 4.1 nm for 0.5 $(Pd/Au)_{at}$ ratio) but not to any significant cluster coalescing.

Surface cleanliness after treating supported clusters in O_3/O_2 at ambient temperature and then in H_2 at 523 K was probed by titration of chemisorbed hydrogen with O_2 (eq 2.1) and by CO chemisorption uptakes. These measurements were carried out on monometallic Pd clusters (0.1% wt) because adsorption stoichiometries have been accurately established only on pure metal surfaces.[28] Evidence for the deprotection of bimetallic Pd–Au clusters is presented by IR-spectroscopy in the next section. Metal dispersions (D) were converted to surface-averaged diameters $\langle d \rangle$ by assuming hemispherical particles ($\langle d \rangle = 0.9/D$; Table 2).[47] The dispersion values and diameters obtained by chemisorption agree well with those estimated from TEM images, consistent with clean surfaces after removal of PVA ligands by O_3/O_2 treatment at ambient temperature.

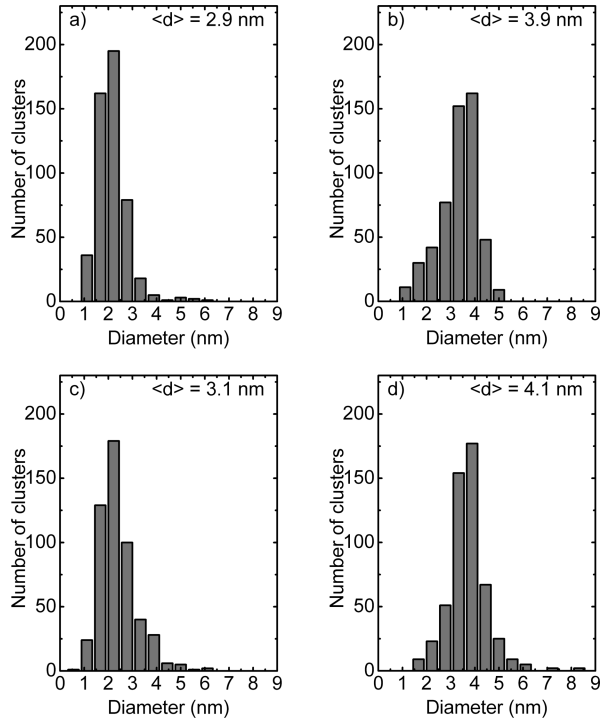

Figure 8. Histograms of supported monometallic Pd clusters (a) and bimetallic $(Pd/Au)_{at} = 0.5$ (b) after deposition; same monometallic Pd (c) and bimetallic sample (d) after an O_3 treatment (89.6 kPa O_2, 6.7 kPa O_3, 3.7 kPa Ar, ambient temperature, 1 h).

Table 2. Dispersion D and Surface-Averaged Diameters $\langle d \rangle$ for O_3-Treated Monometallic Pd Clusters (89.6 kPa O_2, 6.7 kPa O_3, 3.7 kPa Ar, ambient temperature, 1 h) Determined by TEM, Titration of Strongly Bound Hydrogen, and CO Adsorption

	experimental method		
	TEM	titration of hydrogen	CO adsorption
dispersion D (%)	31	32	29
diameter $\langle d \rangle$ (nm)	2.9	2.8	3.1

3.3. Infrared Evidence for Intraparticle Atomic Mobility of Pd and Au upon CO Binding at Ambient Temperature. The displacement–reduction processes described herein would initially lead to outer and inner Pd regions with an intervening Au shell, a structure previously reported for Pd–Au clusters without mechanistic interpretation or spectroscopic evidence for its formation mechanism.[48] Such structures, however, undergo facile restructuring in response to contact with environments that lead to adsorption of species that bind with different strengths on the two bimetallic components.[49,50] The infrared spectra of chemisorbed CO is used here to probe changes in the surface composition of Pd–Au clusters. Clusters were first treated in H_2 (14.3 kPa) at 523 K for 3.6 ks, cooled to 273 K (Section 2.6), and exposed to CO (0.058 kPa CO, 99.942 kPa He). After several infrared spectra were acquired,

dx.doi.org/10.1021/jp500537v | J. Phys. Chem. C 2014, 118, 7468–7479

the temperature was increased to 323 K for 60 s and the sample was then cooled to 273 K to again acquire infrared spectra of chemisorbed CO. Spectra of monometallic and bimetallic ($(Pd/Au)_{at}$ = 1) samples measured by the above-described procedure are shown in Figure 9a and 9b, respectively.

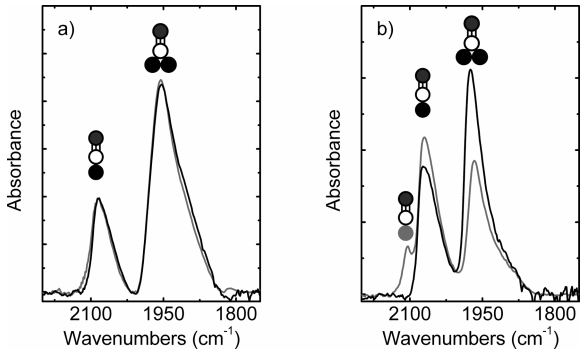

Figure 9. Infrared spectra of CO adsorbed on monometallic Pd at 273 K (0.058 kPa CO, 99.942 kPa He) after reductive pretreatment (523 K, 14.3 kPa H_2, 85.7 kPa Ar) (gray spectrum) and after heating in CO (0.058 kPa CO, 99.942 kPa He) up to 323 K (black spectrum) (a); corresponding spectra (b) on a bimetallic $(Pd/Au)_{at}$ = 1 sample (reductive pretreatment, gray; heating in CO, black). The corresponding CO adsorption modes on Pd (black) or Au (gray) are illustrated above each absorption band.

Monometallic Pd showed two absorption bands assigned to bridge-bound (1955 cm^{-1}) and on-top bound (2084 cm^{-1}) CO (Figure 9a).[51] The spectra before and after heating to 323 K were identical (Figure 9a, gray (before), black (after)). Pd–Au clusters ($(Pd/Au)_{at}$ = 1) (Figure 9b, gray) showed three absorption bands (1966, 2070, and 2105 cm^{-1}) after initial exposure to CO at 273 K. These bands have been assigned to bridge-bound and on-top bound CO on Pd[51] and to linear CO on Au.[52] The ratio of bridge to on-top bound species ($I_{bridge}/I_{on\text{-}top}$) on Pd–Au ($I_{bridge}/I_{on\text{-}top}$ = 0.99) is smaller than that on Pd ($I_{bridge}/I_{on\text{-}top}$ = 3.55) despite their larger size, which leads to the opposite trend on monometallic Pd clusters.[53] These data show instead that Au is present at Pd cluster surfaces, thus decreasing the fraction of the surface that contains vicinal Pd atoms required to form bridge-bound CO species.[52] After the samples are heated to 323 K and cooled to 273 K, the spectra for Pd–Au (Figure 9b, black) lacks the sharp Au–CO band at 2105 cm^{-1} and the ratio of bridge to on-top CO band is larger ($I_{bridge}/I_{on\text{-}top}$ = 1.89) than that upon initial exposure to CO at 273 K ($I_{bridge}/I_{on\text{-}top}$ = 0.99). These data are consistent with the segregation of Pd to the surface of Pd–Au clusters as intraparticle atomic mobility increases with increasing temperature, even at near-ambient conditions.

Bulk Pd–Au systems are exothermic alloys that form single-phase random mixtures for all compositions at temperatures below 900 K.[54] Equimolar compositions have been claimed to form ordered intermetallic compounds below 373 K, but without independent support or confirmed thermodynamic origins.[54,55] However, such bulk properties are not suitable to describe the surface properties of bimetallic systems at the nano scale because the influence of the surface energy becomes dominant. For Pd–Au bulk alloys it has been shown that annealing leads to an enrichment of Au at the surface due the lower surface energy of Au in comparison to that of Pd.[56] The surface composition, however, changes in the presence of adsorbates that bind to Pd more strongly than to Au (e.g., CO), leading to Pd surface enrichment in order to minimize the total free energy of the system.[57] We assume that the heating procedure in H_2 (14.3 kPa, 523 K, 1 h) applied to our bimetallic clusters leads to Au surface enrichment as with the annealing of bulk Pd–Au alloys.[56] Reduction of intraparticle atomic mobility by lowering the temperature to 273 K allows us to demonstrate this Au-enriched surface structure with CO (Figure 9b, gray). Reconstruction upon heating to 323 K, however, forms a Pd-enriched surface (Figure 9b, black) because the binding energy of CO on Pd is stronger than that on Au.

In conclusion, an approach for the preparation of colloidal bimetallic Pd–Au clusters has been presented together with all further preparation steps (deposition, deprotection) required to prepare bimetallic model catalysts. The proposed formation mechanism of the bimetallic clusters may be generally applicable following the thermodynamic guidance that clusters of the less noble metal are exposed to precursors of the nobler metal. The use of preexisting Pd clusters may hence enable the preparation of Pd–Pt, as Pt is more noble than Pd. Similarly, Pt–Au could be obtained by using preexisting Pt clusters. As these three elements are the most noble metals, other metal combinations require the preparation of less noble metal clusters for the use as preexisting clusters in order to apply the proposed mechanism.

4. CONCLUSION

Preparation protocols for colloidal monometallic Pd and bimetallic Pd–Au clusters have been presented using reagents containing only C, H, and O atoms, thus avoiding common surface contaminants that may irreversibly alter the catalytic properties of such bimetallic clusters. It was shown that these clusters can be deposited onto Al_2O_3 and deprotected at ambient temperatures using O_3 without causing any significant cluster coalescence, allowing the application of the presented approach to the preparation of bimetallic model catalysts.

The formation of bimetallic Pd–Au clusters was achieved by addition of the precursor of the second, more noble metal (Au) to preexisting clusters of the first metal (Pd), leading to a sequential displacement–reduction mechanism. This mechanism was proposed to follow the thermodynamic restriction that the preexisting cluster is formed by the less noble metal so that reduction of the more noble metal occurs via galvanic displacement driven by the differences between the electrochemical potentials of the two metals. Furthermore, if monodisperse preexisting clusters are used, bimetallic clusters uniform in chemical composition can be obtained. Fulfilling this thermodynamic restriction may enable the application of the presented formation mechanism in a rational manner to other metal combinations in order to prepare a diverse set of model bimetallic catalysts.

■ ASSOCIATED CONTENT

Supporting Information

TEM images of monometallic Au clusters prepared according to Section 2.1.2, description of the plasmon band deconvolution procedure with an example graph, UV–visible spectra of Pd cluster suspension before and after adsorption of the clusters, temperature-dependent CO_2 evolution rates with corresponding integrated rates of untreated Pd clusters in O_2 with and without traces of O_3 and of an O_3-pretreated Pd cluster sample. This material is available free of charge via the Internet at http://pubs.acs.org.

dx.doi.org/10.1021/jp500537v | J. Phys. Chem. C 2014, 118, 7468–7479

AUTHOR INFORMATION

Corresponding Author

*Tel.: (925) 323-5559. Fax: (510) 642-4778. E-mail: iglesia@berkeley.edu.

Notes

The authors declare no competing financial interest.

ACKNOWLEDGMENTS

S.K. acknowledges the DAAD (Deutscher Akademischer Austauschdienst) for financial support through a postdoc fellowship, Reena Zalpuri for TEM training, and Dr. Dave Flaherty for useful discussions. The authors acknowledge with thanks the financial support for this research from the Director, Office of Basic Energy Sciences, Chemical Sciences Division of the U.S. Department of Energy under Contract DE-AC02-05CH11231. Furthermore, they acknowledge George Meitzner for carefully reading the manuscript and useful suggestions.

REFERENCES

(1) Sinfelt, J. H. *Bimetallic Catalysts: Discoveries, Concepts, and Applications*; Wiley: New York, 1983.

(2) Taylor, K. C. Nitric-oxide Catalysis in Automotive Exhaust Systems. *Catal. Rev.: Sci. Eng.* **1993**, *35* (4), 457−481.

(3) Wolf, R. M.; Siera, J.; Vandelft, F.; Nieuwenhuys, B. E. A Comparative-Study of the Behavior of Single-Crystal Surfaces and Supported Catalysts in No Reduction and Co Oxidation over Pt-Rh Alloys. *Faraday Discuss.* **1989**, *87*, 275−289.

(4) Vielstich, W.; Lamm, A.; Gasteiger, H. *Handbook of Fuel Cells: Fundamentals, Technology, Applications*; Wiley: New York, 2003.

(5) Ponec, V. Alloy catalysts: The concepts. *Appl. Catal., A* **2001**, *222* (1−2), 31−45.

(6) Mavrikakis, M.; Hammer, B.; Norskov, J. K. Effect of strain on the reactivity of metal surfaces. *Phys. Rev. Lett.* **1998**, *81* (13), 2819−2822.

(7) Besenbacher, F.; Chorkendorff, I.; Clausen, B. S.; Hammer, B.; Molenbroek, A. M.; Norskov, J. K.; Stensgaard, I. Design of a surface alloy catalyst for steam reforming. *Science* **1998**, *279* (5358), 1913−1915.

(8) Mihut, C.; Descorme, C.; Duprez, D.; Amiridis, M. D. Kinetic and spectroscopic characterization of cluster-derived supported Pt-Au catalysts. *J. Catal.* **2002**, *212* (2), 125−135.

(9) Sachdev, A.; Schwank, J. Microstructure and Reactivity of Supported Bimetallic Platinum Gold Catalysts. *J. Catal.* **1989**, *120* (2), 353−369.

(10) Rebelli, J.; Detwiler, M.; Ma, S. G.; Williams, C. T.; Monnier, J. R. Synthesis and characterization of Au-Pd/SiO_2 bimetallic catalysts prepared by electroless deposition. *J. Catal.* **2010**, *270* (2), 224−233.

(11) Schaal, M. T.; Pickerel, A. C.; Williams, C. T.; Monnier, J. R. Characterization and evaluation of Ag-Pt/SiO_2 catalysts prepared by electroless deposition. *J. Catal.* **2008**, *254* (1), 131−143.

(12) Toshima, N.; Kushihashi, K.; Yonezawa, T.; Hirai, H. Colloidal Dispersions of Palladium-Platinum Bimetallic Clusters Protected by Polymers: Preparation and Application to Catalysis. *Chem. Lett.* **1989**, *10*, 1769−1772.

(13) Toshima, N.; Yonezawa, T. Bimetallic nanoparticles—Novel materials for chemical and physical applications. *New J. Chem.* **1998**, *22* (11), 1179−1201.

(14) Wang, X. D.; Stover, J.; Zielasek, V.; Altmann, L.; Thiel, K.; Al-Shamery, K.; Baumer, M.; Borchert, H.; Parisi, J.; Kolny-Olesiak, J. Colloidal Synthesis and Structural Control of PtSn Bimetallic Nanoparticles. *Langmuir* **2011**, *27* (17), 11052−11061.

(15) Ahrenstorf, K.; Heller, H.; Kornowski, A.; Broekaert, J. A. C.; Weller, H. Nucleation and Growth Mechanism of Ni_xPt_{1-x} Nanoparticles. *Adv. Funct. Mater.* **2008**, *18* (23), 3850−3856.

(16) Alayoglu, S.; Zavalij, P.; Eichhorn, B.; Wang, Q.; Frenkel, A. I.; Chupas, P. Structural and Architectural Evaluation of Bimetallic Nanoparticles: A Case Study of Pt−Ru Core−Shell and Alloy Nanoparticles. *ACS Nano* **2009**, *3* (10), 3127−3137.

(17) Zheng, N. F.; Stucky, G. D. A general synthetic strategy for oxide-supported metal nanoparticle catalysts. *J. Am. Chem. Soc.* **2006**, *128* (44), 14278−14280.

(18) Miedziak, P.; Sankar, M.; Dimitratos, N.; Lopez-Sanchez, J. A.; Carley, A. F.; Knight, D. W.; Taylor, S. H.; Kiely, C. J.; Hutchings, G. J. Oxidation of benzyl alcohol using supported gold-palladium nanoparticles. *Catal. Today* **2011**, *164* (1), 315−319.

(19) Choi, M.; Wu, Z. J.; Iglesia, E. Mercaptosilane-Assisted Synthesis of Metal Clusters within Zeolites and Catalytic Consequences of Encapsulation. *J. Am. Chem. Soc.* **2010**, *132* (26), 9129−9137.

(20) Jaska, C. A.; Clark, T. J.; Clendenning, S. B.; Grozea, D.; Turak, A.; Lu, Z. H.; Manners, I. Poisoning of heterogeneous, late transition metal dehydrocoupling catalysts by boranes and other group 13 hydrides. *J. Am. Chem. Soc.* **2005**, *127* (14), 5116−5124.

(21) Vig, J. R. UV Ozone Cleaning of Surfaces. *J. Vac. Sci. Technol., A* **1985**, *3* (3), 1027−1034.

(22) Aliaga, C.; Park, J. Y.; Yamada, Y.; Lee, H. S.; Tsung, C. K.; Yang, P. D.; Somorjai, G. A. Sum Frequency Generation and Catalytic Reaction Studies of the Removal of Organic Capping Agents from Pt Nanoparticles by UV−Ozone Treatment. *J. Phys. Chem. C* **2009**, *113* (15), 6150−6155.

(23) Mayrhofer, K. J. J.; Juhart, V.; Hartl, K.; Hanzlik, M.; Arenz, M. Adsorbate-Induced Surface Segregation for Core-Shell Nanocatalysts. *Angew. Chem., Int. Ed.* **2009**, *48* (19), 3529−3531.

(24) Gao, F.; Wang, Y.; Goodman, D. W. CO Oxidation over AuPd(100) from Ultrahigh Vacuum to Near-Atmospheric Pressures: CO Adsorption-Induced Surface Segregation and Reaction Kinetics. *J. Phys. Chem. C* **2009**, *113* (33), 14993−15000.

(25) Tao, F.; Grass, M. E.; Zhang, Y. W.; Butcher, D. R.; Renzas, J. R.; Liu, Z.; Chung, J. Y.; Mun, B. S.; Salmeron, M.; Somorjai, G. A. Reaction-Driven Restructuring of Rh-Pd and Pt-Pd Core-Shell Nanoparticles. *Science* **2008**, *322* (5903), 932−934.

(26) Yonezawa, T.; Toshima, N. Mechanistic Consideration of Formation of Polymer-Protected Nanoscopic Bimetallic Clusters. *J. Chem. Soc., Faraday Trans.* **1995**, *91* (22), 4111−4119.

(27) Mirth, G.; Eder, F.; Lercher, J. A. Design and Application of a New Reactor for In-situ Infrared Spectroscopic Investigations of Heterogeneously Catalyzed Reactions. *Appl. Spectrosc.* **1994**, *48* (2), 194−197.

(28) Benson, J. E.; Hwang, H. S.; Boudart, M. Hydrogen-Oxygen Titration Method for Measurement of Supported Palladium Surface Areas. *J. Catal.* **1973**, *30* (1), 146−153.

(29) Zilm, K. W.; Bonneviot, L.; Haller, G. L.; Han, O. H.; Kermarec, M. ^{13}C NMR Spectra of ^{13}CO Adsorbed on Silica-Supported Palladium Particles: Particle Size Dependence of the Surface Diffusion Rate and the ^{13}C Knight Shift. *J. Phys. Chem.* **1990**, *94* (23), 8495−8498.

(30) Hoffmann, F. M. Infrared reflection-absorption spectroscopy of adsorbed molecules. *Surf. Sci. Rep.* **1983**, *3* (2−3), 107−192.

(31) Gilbert, R. G.; Hess, M.; Jenkins, A. D.; Jones, R. G.; Kratochvil, R.; Stepto, R. F. T. Dispersity in polymer science (IUPAC Recommendations 2009) (vol 81, pg 351, 2009). *Pure Appl. Chem.* **2009**, *81* (4), 779−779.

(32) *Handbook of Chemistry and Physics*, 91st ed.; Haynes, W. M., Ed.; CRC Press: Boca Raton, FL, 2010.

(33) Lang, H. G.; Maldonado, S.; Stevenson, K. J.; Chandler, B. D. Synthesis and characterization of dendrimer templated supported bimetallic Pt-Au nanoparticles. *J. Am. Chem. Soc.* **2004**, *126* (40), 12949−12956.

(34) Scott, R. W. J.; Wilson, O. M.; Oh, S. K.; Kenik, E. A.; Crooks, R. M. Bimetallic palladium-gold dendrimer-encapsulated catalysts. *J. Am. Chem. Soc.* **2004**, *126* (47), 15583−15591.

(35) Toshima, N.; Harada, M.; Yamazaki, Y.; Asakura, K. Catalytic Activity and Structural Analysis of Polymer-Protected Au/Pd Bimetallic Clusters Prepared by the Successive Reduction of $HAuCl_4$ and $PdCl_2$. *J. Phys. Chem.* **1992**, *96* (24), 9927−9933.

(36) Kreibig, U. *Optical Properties of Metal Clusters*. Springer-Verlag: Berlin, 1995.
(37) Mie, G. Articles on the optical characteristics of turbid tubes, especially colloidal metal solutions. *Ann. Phys. (Berlin, Ger.)* **1908**, *25* (3), 377−445.
(38) Kreibig, U.; Genzel, L. Optical-Absorption of Small Metallic Particles. *Surf. Sci.* **1985**, *156*, 678−700.
(39) Ghosh, S. K.; Nath, S.; Kundu, S.; Esumi, K.; Pal, T. Solvent and ligand effects on the localized surface plasmon resonance (LSPR) of gold colloids. *J. Phys. Chem. B* **2004**, *108* (37), 13963−13971.
(40) Link, S.; El-Sayed, M. A. Size and temperature dependence of the plasmon absorption of colloidal gold nanoparticles. *J. Phys. Chem. B* **1999**, *103* (21), 4212−4217.
(41) Henglein, A. Colloidal palladium nanoparticles: Reduction of Pd(II) by H_2; $Pd_{core}Au_{shell}Ag_{shell}$ particles. *J. Phys. Chem. B* **2000**, *104* (29), 6683−6685.
(42) Zhao, M. Q.; Crooks, R. M. Intradendrimer exchange of metal nanoparticles. *Chem. Mater.* **1999**, *11* (11), 3379−3385.
(43) Kan, C. X.; Cai, W. P.; Li, C. C.; Zhang, L. D.; Hofmeister, H. Ultrasonic synthesis and optical properties of Au/Pd bimetallic nanoparticles in ethylene glycol. *J. Phys. D: Appl. Phys.* **2003**, *36* (13), 1609−1614.
(44) Brodnyan, J. G. Emulsion Particle Size III. Particle Size Distributions determined by various Growth Mechanisms. *J. Colloid Sci.* **1960**, *15*, 573−577.
(45) Goodrich, F. C. Nucleation Rates + Kinetics of Particle Growth. I. Pure Birth Process. *Proc. R. Soc. London, Ser. A* **1964**, *277* (1368), 155−166.
(46) Singman, C. N. Atomic Volume and Allotropy of the Elements. *J. Chem. Educ.* **1984**, *61* (2), 137−142.
(47) Boudart, M.; Djega-Mariadassou, G. *Kinetics of Heterogeneous Catalytic Reactions*. Princeton University Press: Princeton, NJ, 1984.
(48) Ferrer, D.; Torres-Castro, A.; Gao, X.; Sepulveda-Guzman, S.; Ortiz-Mendez, U.; Jose-Yacaman, M. Three-layer core/shell structure in Au−Pd bimetallic nanoparticles. *Nano Lett.* **2007**, *7* (6), 1701−1705.
(49) Cadenhea, Da; Wagner, N. J. Low-Temperature Hydrogen Adsorption on Copper−Nickel Alloys. *J. Phys. Chem.* **1968**, *72* (8), 2775−2781.
(50) Vanderpl, P.; Sachtler, W. M. Interaction of Benzene with Protium and Deuterium on Copper-Nickel Films with Known Surface Composition. *J. Catal.* **1968**, *12* (1), 35−44.
(51) Eischens, R. P.; Pliskin, W. A. The Infrared Spectra of Adsorbed Molecules. *Adv. Catal.* **1958**, *10*, 1−56.
(52) Kugler, E. L.; Boudart, M. Ligand and ensemble effects in the adsorption of carbon monoxide on supported palladium-gold alloys. *J. Catal.* **1979**, *59* (2), 201−210.
(53) Sheu, L. L.; Karpinksi, Z.; Sachtler, W. M. H. Effects of Palladium Particle Size and Palladium Silicide Formation on Fourier Transform Infrared Spectra of CO Adsorbed on Pd/SiO_2 Catalysts. *J. Phys. Chem.* **1989**, *93* (12), 4890−4894.
(54) Okamoto, H.; Massalski, T. The Au-Pd (Gold-Palladium) system. *J. Phase Equilib.* **1985**, *6* (3), 229−235.
(55) Lin, W.; Spruiell, J. E.; Williams, R. O. Sort-Range Order in a Gold-40.0 Atomic Percent Palladium Alloy. *J. Appl. Crystallogr.* **1970**, *3* (OCT1), 297−305.
(56) Jablonski, A.; Overbury, S. H.; Somorjai, G. A. The surface composition of the gold-palladium binary alloy system. *Surf. Sci.* **1977**, *65* (2), 578−592.
(57) Gao, F.; Wang, Y. L.; Goodman, D. W. CO Oxidation over AuPd(100) from Ultrahigh Vacuum to Near-Atmospheric Pressures: CO Adsorption-Induced Surface Segregation and Reaction Kinetics. *J. Phys. Chem. C* **2009**, *113* (33), 14993−15000.